Analysis of ECG Signals by Dynamic Mode Decomposition

Honorine Niyigena Ingabire, Kangjia Wu, Joan Toluwani Amos, Sixuan He, Xiaohang Peng, Wenan Wang, Min Li, Jinying Chen, Yukun Feng, Nini Rao, and Peng Ren

***Abstract*— Objective: Based on cybernetics, a large system can be divided into subsystems, and the stability of each can determine the overall properties of the system. However, this stability analysis perspective has not yet been employed in electrocardiogram (ECG) signals. This is the first study to attempt to evaluate whether the stability of decomposed ECG subsystems can be analyzed in order to effectively investigate the overall performance of ECG signals, and aid in disease diagnosis. Methods: We used seven different cardiac pathologies (myocardial infarction, cardiomyopathy, bundle branch block, dysrhythmia, hypertrophy, myocarditis, and valvular heart disease) to illustrate our method. Dynamic mode decomposition (DMD) was first used to decompose ECG signals into dynamic modes (DMs) which can be regarded as ECG subsystems. Then, the features related to the DMs stabilities were extracted, and nine common classifiers were implemented for classification of these pathologies. Results: Most features were significant for differentiating the above-mentioned groups (*p* value<0.05 after Bonferroni correction). In addition, our method outperformed all existing methods for cardiac pathology classification. Conclusion: We have provided a new spatial and temporal decomposition method, namely DMD, to study ECG signals. Significance: Our method can reveal new cardiac mechanisms, which can contribute to the comprehensive understanding of its underlying mechanisms and disease diagnosis, and thus, can be widely used for ECG signal analysis in the future.**

***Index Terms*— Cardiac pathologies, Dynamic mode decomposition (DMD), electrocardiogram (ECG), multi-lead ECG, stability, subsystems.**

I. Introduction

A. Stability Analysis of ECG Signals

ELECTROCARDIOGRAM (ECG) is an important tool to capture the electrical activity of the heart over time. Conductive electrodes are selectively placed on the body's surface to capture the small electrical changes that occur as a result of depolarization and repolarization of the cardiac muscle over each heartbeat (cardiac cycle) [1]. These changes reflect a series of waves, P, Q, R, S, and T waves. The electrical potential difference between a pair of electrodes during each cardiac cycle is graphically represented as a lead. The standard ECG is comprised of 12-leads including bipolar limb leads (I, II, and III) and unipolar leads (augmented limb leads i.e. aVR, aVL, and aVF, and precordial chest leads i.e. V1, V2, V3, V4, V5, and V6). The 12-lead ECG reflects the 3-dimensional electrical activity of the heart captured from 12 different viewpoints (or leads). These leads reflect the electrical activity of different anatomic areas of the heart.

Cardiac diseases, such as myocardial infarction (MI), cardiomyopathy (CM), bundle branch block (BBB), hypertrophy (HT), and valvular heart disease (VHD), have been widely diagnosed by monitoring 12-lead ECG changes [2]–[4]. Analysis of a single-lead ECG signal has low computational cost and is more easily interpretable than 12-lead ECG signals. However, 12-lead ECG has many advantages: (1) It can fully capture signs of cardiac abnormalities located in any anatomic area of the heart, contributing to cardiac disease diagnosis. (2) It can fully reflect the underlying dynamics of the heart by providing comprehensive information about its activities. This paper regards the heart as a complex large-scale system, and its dynamic behaviors are captured from 12-lead ECG signals in macroscopic quantities. Since single-lead ECG only captures limited information on heart mechanisms, therefore, 12-lead ECG signals were used for further analysis.

Stability analysis is an important issue in cybernetics (or system science) with many applications across fields, such as power systems, product design, and industrial manufacturing [5]–[8]. Recently, it has received increased attention in the life science. Previous studies have also revealed that the health status of individuals can be reflected in instability of their physiological signals, including blood oxygen saturation, respiration, and electroencephalography signals. For example, analysis of the stability of physiological signals, such as the heart rate, respiration, and blood oxygen saturation of a patient with sleep apnea led to the successful extraction of abnormal breathing patterns [9]. Similarly, Hocepied *et al*. found that electroencephalography signals of epileptic patients are less stable compared with those of healthy individuals [10]. According to these findings, Glass *et al.* concluded that most pathological conditions can be reflected in the instability of

This work was sponsored by the National Natural Science Foundation of China (Grant number: 62171109, 61872405), the Key R&D Project of Sichuan Province (Grant number: 2020YFS0094, 2020YFS0243), and by University of Electronic Science and Technology of China. Corresponding authors: {Nini Rao, Peng Ren}.

H. Niyigena Ingabire, K. Wu, J. Toluwani Amos, S. He, X. Peng, W. Wang, M. Li, J. Chen, Y. Feng, N. Rao and P. Ren are with the department of Biomedical Engineering, University of Electronic Science and Technology of China, Chengdu 610054, China.

physiological signals [11]. Apart from this, it should also be noted that according to cybernetics, the overall performance of a large-scale system can be determined by the stability of many subsystems decomposed from it [12]. As mentioned above, in this study, the heart is regarded as a complex large system with dynamic behaviors which can be reflected and measured by multi-lead ECG signals. Thus, it is essential to evaluate how the stability of decomposed ECG subsystems affects the overall properties of multi-lead ECG signals from subjects suffering from diseases. This perspective has not yet been evaluated by previous studies.

Finally, it must be noted that some previous studies evaluated the stability of ECG signals based on the variability of different ECG waves, such as the T-wave and QT-interval [13]. However, this study refers to the stability of ECG signals from system science theory, which has an entirely different physiological meaning from the previous studies (see the Methods section for more details). We attempt to use a novel approach, namely dynamic mode decomposition (DMD), to demonstrate the effectiveness of our perspective for analyzing ECG signals.

B. Dynamic Mode Decomposition

DMD is a powerful new decomposition method capable of capturing coherent spatial-temporal patterns from complex data by assuming that the spatial pattern of the observed data at each time point is given by a linear combination of spatial patterns at previous time points [14]. This method was initially implemented for the analysis of fluid flows [15]. It is a data-driven approach, which does not require any governing equation or prior assumptions of underlying system dynamics. In addition, it encompasses the ability of both singular value decomposition (to extract inherent modes from high-dimensional data) and spectral analysis (to assess oscillatory frequencies correspond to those inherent modes). For these reasons, DMD has recently been used to analyze high-dimensional and dynamic physiological signals and public health data, such as epidemiological data, brain-related signals, and others. For instance, DMD was successfully employed to interpret the spread of three infectious diseases, using flu activity data provided by Google's Flu Trends tool, pre-vaccination measles from the UK, and type-1 paralytic polio cases in Nigeria [16]. Furthermore, Brunton *et al*. used DMD to analyze large-scale sleeping electrocorticography data, and were successful in detecting spindle networks during sleep [17]. Similarly, Solaija *et al*. used DMD to accurately detect epileptic seizures of electroencephalography signals, and Casorso et *al.* also used this method to analyze resting-state and motor-task function magnetic resonance imaging data to model the brain's spatial-temporal organization [18], [19]. However, it has not yet been used to analyze multi-lead ECG data, which is also dynamic and high-dimensional. In addition, in contrast to other traditional data decomposition methods, such as principal component analysis (PCA), empirical mode decomposition (EMD), and wavelet transform (WT), only DMD can decompose complex (high-dimensional and dynamic) data into subsystems, namely dynamic modes (DMs), with degree of stability. Therefore, this study attempts to analyze ECG signals based on stable and unstable DMs from multi-lead ECG signals. This approach may not only aid in revealing new cardiac dynamic mechanisms, but also contribute to research on heart-related diseases.

C. Cardiac Abnormalities

We evaluated our approach using the ECG signals of patients with various cardiac abnormalities, such as MI, CM, BBB, HT, VHD, and myocarditis (MCD). MI, also known as heart attack, is the most severe cardiovascular disease and one of the top causes of mortality in the world. Every year, more than 8 million people die globally from MI [20]. It occurs as a result of necrosis of heart cells and permanent damage of the heart muscle due to prolonged insufficient oxygen supply (ischemia), which is caused by narrowed coronary arteries. This can lead to both acute infarction and sudden death [4]. MI characteristics are captured by monitoring ECG changes, including ST-segment elevation and depression, P-wave, T-wave, and QRS-complex abnormalities [4]. Dysrhythmia (DT) occurs as the result of problems in the electrical conduction system. Cardiac muscle diseases including CM and HT are characterized by the presence of T-wave inversion, ST-segment depression, and deep T-wave inversion in leads I, II, aVL, aVF, V4, V5, and V6. In VHD, the heart valves do not close or open properly. MCD occurs when there is inflammation of the myocardium (heart muscle), which is as a result of the immune response to infections. BBB occurs due to delays in the heart conduction process. The characteristics of right BBB include the presence of wide R-wave and S-wave in the leads V1 and V6 [2]. For left BBB, the amplitude of the R-wave and the duration of the QRS complex are high, and the T-wave inversion is present in the precordial leads [2].

The aforementioned pathologies have been detected using various approaches, including time-domain, WT, discrete Fourier transform (DFT), discrete cosine transform, PCA, EMD, and neural network methods [13], [21]–[32]. For example, Sadhukhan *et al*. extracted the phases after implementing DFT on ECG signals for MI detection [22]. Acharya *et al*. used three types of coefficients based on discrete wavelet transform, discrete cosine transform, and EMD for the detection of MI [23]. In addition, Reasat and Shahnaz, and Liu *et al.*, implemented different types of neural networks for MI detection [33], [34]. Tripathy *et al*. implemented principal component multivariate multiscale sample entropy for detection and classification of MI, CT, DT, and HT [35]. In [36], BBB was detected based on a complex wavelet sub-band dual-spectrum. Jain and Bhaumik applied a specific signal processing technique for integrated circuits on ECG signals for HT, DT, and BBB detection [37].

Meanwhile, different approaches have been proposed for multiclass ECG classification [35], [38]–[40]. For example, Deng *et al*. and Dey *et al*., respectively used convolution neural network (CNN) for eight classes of ECG (HC, MI, BBB, CT, DT, HT, MC, and VHD) and three classes of ECG (HC, MI, and non-MI) classification [39], [40]. This study attempts to implement DMD to analyze ECG signals in order to improve classification of binary-class and multi-class ECG signals. Specifically, our proposed method was evaluated on

different types of binary-class ECG signals (MI versus normal ECG signals, BBB versus normal ECG signals, CT versus normal ECG signals, DT versus normal ECG signals, and HT versus normal ECG signals) and classification of eight-class ECG signals, including HC, MI, BBB, CT, DT, HT, MCD, and VHD.

The flowchart of this study is shown in Fig. 1. First, the multi-lead ECG data was preprocessed in order to remove artifacts, and further segmented into ECG beats and frames. Each individual beat and frame signal were then decomposed into DMs using the DMD algorithm. Then, eigenvalues were used to determine whether their corresponding DMs were either stable or unstable. After, the features related to the stability of these DMs were extracted, and the statistical tests were performed on each feature to assess the differences between the stability changes of DMs of ECG beats and frames of patients with different cardiac abnormalities and HCs. Last, classification performance was evaluated via nine common classifiers.

II. Methods

This study used Physikalisch-Technische Bundesanstalt (PTB), a well-known public diagnostic ECG database provided by the national metrology institute of the Federal Republic of Germany, for analysis [41]. The PTB ECG database contains digitized ECG recordings from 148 MI patients, 15 BBB patients, 18 CT patients, 14 DT patients, 7 HT patients, 4 MC patients, 6 VHD patients, and 52 HCs with an average age of 57.2 years. Each ECG time series was recorded by the 12 standard leads (I, II, III, aVR, aVL, aVF, V1, V2, V3, V4, V5, V6). The duration of each recording was approximately 2 minutes, and each ECG signal was sampled at 1000 Hz with a 16-bit resolution over a range of ±16.384 mV.

In the section below, we demonstrate the proposed method to analyze multi-lead ECG signals to detect of cardiovascular pathologies. The detection block (see Fig.1) consists of preprocessing, feature extraction based on DMD, and classification.

A. Preprocessing

The preprocessing includes filtering and beat segmentation. For filtering, artifacts such as noise and baseline wander were filtered out by the Daubechies wavelet basis function, and powerline interference was removed by a second-order notch filter, then a fourth-order butterworth low pass filter with a cutoff frequency of 100 Hz was used to reduce very high-frequency content [42]. These preprocessing techniques have been applied by different studies for ECG analysis and are effective in filtering different artifacts, including motion and baseline wander.

For beat segmentation, the R-wave is considered as a distinctive point due to its high amplitude and clearly visible peak. The Pan-Tompkins algorithm has been widely used for R-peak detection [43]. We used this algorithm similarly to identify the R-peaks. Once the R-peaks were identified, a multi-lead segment of 651 time points, including 250 points before the R-peak, and 400 points after, was considered as the ECG beat. This beat length was chosen because it has been

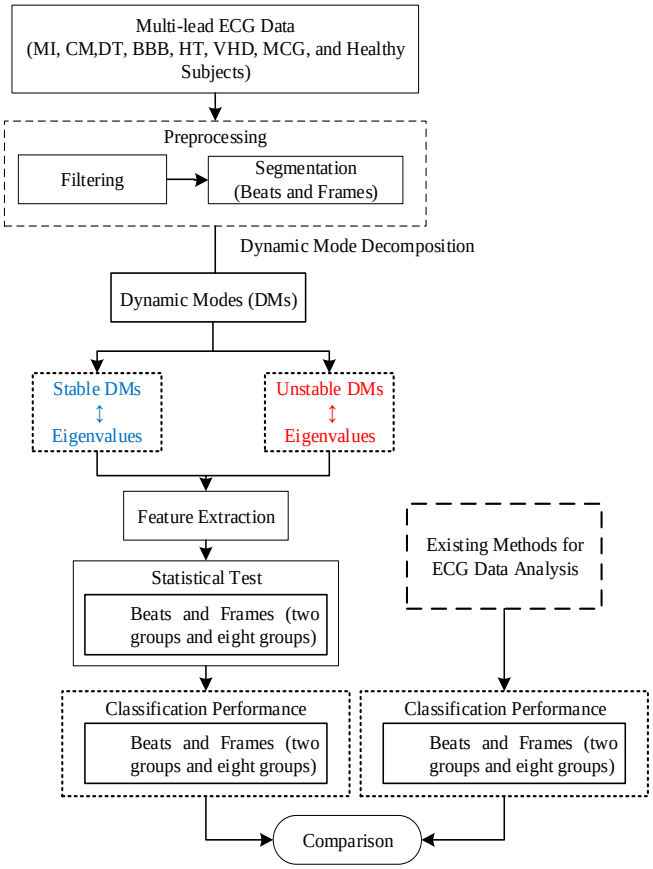

Fig. 1. The flow chart of this study. Note: classification performance includes accuracy, precision, recall, and area under the curve (AUC) values.

employed in previous studies which used the PTB database [23], [31]. These studies have demonstrated that this length generally contains a large proportion of information on the heartbeat, and can be successfully used to detect ECG beats for different individuals. It should be noted that to avoid inconsistency in beat length, the first and last beats of each subject were not considered.

The aforementioned pathologies, such as DT (ventricular arrhythmia, supraventricular arrhythmia, premature ventricular ectopic beats, and sinus arrhythmia), HT, and BBB, are mainly diagnosed using frame-based processing; in other words, beat segmentation is not required during preprocessing [44]. In this way, during preprocessing, multi-lead ECG signals were segmented into non-overlapping frames of 4096 time points (4.096 seconds). This frame size was chosen by following the previous studies which used the PTB database [30], [35], [36], [38]. Thus, in order to easily compare our proposed method with those of existing studies that used either beat-based or frame-based processing, both processing methods were considered. After preprocessing, the multi-lead ECG signal features were extracted using DMD.

B. Dynamic Mode Decomposition

DMD is a powerful decomposition approach that is used to evaluate dynamic systems with high-dimensional data. The DMD algorithm has the benefit of decomposing time series

data into a set of DMs that contain spatial and temporal patterns. Tu *et al.* has refined the definition of DMD algorithm, as shown below [45]. Let us consider two $n\times(k-1)$ raw data matrices $\mathbf{X}$ and $\mathbf{X}^s$, whose rows and columns respectively denote the leads and sampling points of ECG beats. In the case of 12-lead ECG signals, n is equal to 12. These matrices can be constructed by arranging measurements from k sampling time points as follows:

$$\mathbf{X}=\begin{pmatrix} x_{11} & \cdots & x_{1(k-1)} \\ \vdots & \ddots & \vdots \\ x_{n1} & \cdots & x_{n(k-1)} \end{pmatrix}=\begin{bmatrix}\mathbf{x}_1 & \cdots & \mathbf{x}_{k-1}\end{bmatrix} \tag{1}$$

$$\mathbf{X}^s=\begin{pmatrix} x_{12} & \cdots & x_{1k} \\ \vdots & \ddots & \vdots \\ x_{n2} & \cdots & x_{nk} \end{pmatrix}=\begin{bmatrix}\mathbf{x}_2 & \cdots & \mathbf{x}_k\end{bmatrix} \tag{2}$$

where columns (or snapshots) of $\mathbf{X}^s$ are obtained by shifting those in $\mathbf{X}$ by one time point, therefore the data in these matrices largely overlap.

DMD assumes that the temporal progression from $\mathbf{X}$ to $\mathbf{X}^s$ is governed by a linear operator $\mathbf{A}$, which satisfies the following relationship:

$$\mathbf{X}^s=\mathbf{A}\mathbf{X} \tag{3}$$

Linear regression of the non-linear dynamics between these consecutive data matrices, i.e. $\mathbf{X}$ and $\mathbf{X}^s$, can be determined by estimating the eigendecomposition of this operator $\mathbf{A}$ based on one possible approach, which is to calculate the pseudoinverse of $\mathbf{X}$ using its SVD.

It is important to note that the snapshots in the data matrix $\mathbf{X}$ are assumed to be high dimensional, i.e. if the measurements n of a snapshot are larger than the total number of snapshots $k-1$, then the transition matrix $\mathbf{A}$ (with the size $n\times n$) may be high dimensional. As a result, it may not be straightforward to compute the eigendecomposition of $\mathbf{A}$. Thus, instead of calculating $\mathbf{A}$ directly, the DMD algorithm uses a reduced matrix $\tilde{\mathbf{A}}$ given by projecting $\mathbf{A}$ onto the leading singular vectors of $\mathbf{X}$ to compute the eigendecomposition of $\mathbf{A}$ using the following procedure:

Step 1. Determine the SVD of the first data matrix:

$$\mathbf{X}\approx\mathbf{U}\mathbf{\Sigma}\mathbf{V}^* \tag{4}$$

Then, substitute (4) into (3) to get the SVD of $\mathbf{X}^s$:

$$\mathbf{X}^s=\mathbf{A}\mathbf{U}\mathbf{\Sigma}\mathbf{V}^* \tag{5}$$

where $\mathbf{U}$, $\mathbf{\Sigma}$, and $\mathbf{V}$ represent left singular vectors, singular values, and right singular vectors, respectively.

Step 2. Compute the pseudo-inverse of $\mathbf{X}$ to get the matrix $\mathbf{A}$:

$$\mathbf{A}=\mathbf{X}^s\mathbf{X}^{-1}=\mathbf{X}^s\mathbf{V}\mathbf{\Sigma}^{-1}\mathbf{U}^* \tag{6}$$

Step 3. Project $\mathbf{A}$ onto the proper orthogonal decomposition modes of $\mathbf{U}$ to get $\tilde{\mathbf{A}}$:

$$\tilde{\mathbf{A}}=\mathbf{U}^*\mathbf{A}\mathbf{U}=\mathbf{U}^*\mathbf{X}^s\mathbf{V}\mathbf{\Sigma}^{-1} \tag{7}$$

Step 4. The eigendecomposition of $\tilde{\mathbf{A}}$ is calculated as follows:

$$\tilde{\mathbf{A}}\mathbf{W}=\mathbf{W}\mathbf{\Lambda} \tag{8}$$

where the columns of $\mathbf{W}$ are the eigenvectors of $\tilde{\mathbf{A}}$, and the elements λ_i of the diagonal matrix $\mathbf{\Lambda}$ are the eigenvalues of the full matrix $\mathbf{A}$, which are also the DMD eigenvalues of data $\mathbf{X}$.

Step 5. Compute the DMs $\mathbf{\Phi}$ of $\mathbf{X}$ using the eigenvectors $\mathbf{W}$ and time-shifted snapshot matrix $\mathbf{X}^s$:

$$\mathbf{\Phi}=\mathbf{X}^s\mathbf{V}\mathbf{\Sigma}^{-1}\mathbf{W} \tag{9}$$

It should be noted that these DMs $\mathbf{\Phi}$ denote the eigenvectors of the high-dimensional operator $\mathbf{A}$, and each DM $\boldsymbol{\phi}_i$ corresponds to an eigenvalue λ_i given by $\mathbf{\Lambda}$ as shown in Tu *et al.* [45].

Finally, the observed data can be approximately constructed as the simple dynamic model $\widehat{\mathbf{X}}(t)$:

$$\mathbf{X}(t)\approx\widehat{\mathbf{X}}(t)=\mathbf{\Phi}\exp(\mathbf{\Omega}t)\mathbf{b} \tag{10}$$

where $\mathbf{\Omega}=\log(\mathbf{\Lambda})/\Delta t$ is a diagonal matrix containing eigenvalues in continuous time, t is time, Δt is the time difference between two consecutive points, and $\mathbf{b}$ is a vector containing a set of weights to match the initial time point measured, such that $\mathbf{b}=\mathbf{\Phi}^{-1}\mathrm{X}_1$.

The essence of the above algorithm is to decompose data arranged, as in (1) into a set of coupled spatial-temporal patterns. Note that both $\mathbf{\Phi}$ and $\mathbf{\Lambda}$ are complex values. Fig. 4 shows an example of one stable and unstable DMs for a single ECG beat (each DM contains real and imaginary parts). An eigenvalue can be expressed as $\lambda_i=r_i^{j\omega_i}$, where r_i denotes the damping ratio and ω_i (element of $\mathbf{\Omega}$) denotes the frequency of $\boldsymbol{\phi}_i$. The oscillatory frequency F_i of each DM can be determined by the imaginary part of ω_i as follows:

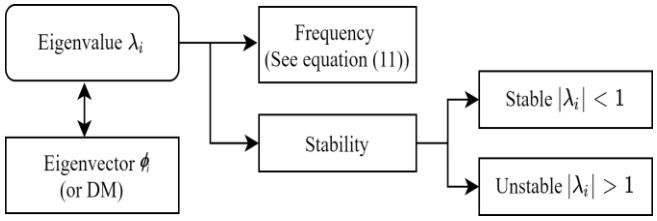

Fig. 2. The procedures to compute the stability of DMs and their corresponding frequencies.

$$F_i = \frac{\text{imag}(\omega_i)}{2\pi} \tag{11}$$

According to the theory of discrete-time linear systems, the magnitude of eigenvalue $|\lambda_i|$ indicates the stability of the system, where the system is considered as asymptotically stable when $|\lambda_i| < 1$. However, if $|\lambda_i| > 1$, the system is considered unstable [46]. Therefore, the stability and frequency of each DM can be indicated by its corresponding eigenvalue (see Fig. 2) [47]. The stable and unstable DMs of a 12-lead ECG signal and their corresponding eigenvalues are shown as follows:

$$\boldsymbol{\Phi} = \left[\boldsymbol{\Phi}^u \ , \boldsymbol{\Phi}^s \right] \quad \Leftrightarrow \quad \boldsymbol{\Lambda} = \begin{bmatrix} \boldsymbol{\Lambda}^u & 0 \\ 0 & \boldsymbol{\Lambda}^s \end{bmatrix} \tag{12}$$

where $\boldsymbol{\Phi}^u$ is the matrix containing unstable DMs, and $\boldsymbol{\Lambda}^u$ is the diagonal matrix containing their corresponding eigenvalues, as follows:

$$\boldsymbol{\Phi}^u = \left[\boldsymbol{\phi}_1^u \ , \ldots, \boldsymbol{\phi}_d^u, \ldots, \boldsymbol{\phi}_D^u \right] \tag{13}$$

$$\boldsymbol{\Lambda}^u = \begin{bmatrix} \lambda_1^u & 0 & \cdots & \cdots & 0 \\ 0 & \ddots & 0 & 0 & \vdots \\ \vdots & 0 & \lambda_d^u & 0 & \vdots \\ \vdots & 0 & 0 & \ddots & 0 \\ 0 & \cdots & \cdots & 0 & \lambda_D^u \end{bmatrix} \tag{14}$$

where $\boldsymbol{\phi}_d^u$ is a vector which represents unstable DM, and λ_d^u is an element which denotes its corresponding eigenvalue, where $d = 1,2,\ldots,D$, and D denotes the total number of unstable DMs. Each element of unstable DM $\boldsymbol{\phi}_d^u$, namely $\boldsymbol{\phi}_d^u(l)$, corresponds to each lead where $l = 1,2,\ldots,12$. $\boldsymbol{\Phi}^s$ is the matrix containing stable DMs, and $\boldsymbol{\Lambda}^s$ is the diagonal matrix containing their corresponding eigenvalues, as follows:

$$\boldsymbol{\Phi}^s = \left[\boldsymbol{\phi}_1^s \ , \ldots, \boldsymbol{\phi}_c^s, \ldots, \boldsymbol{\phi}_C^s \right] \tag{15}$$

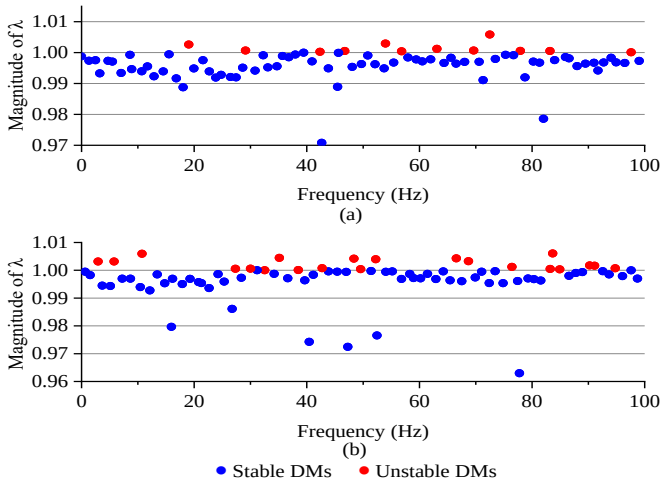

Fig. 3. The magnitudes and oscillatory frequencies of eigenvalues of DMs for one ECG beat. (a) Healthy control (HC); and (b) Myocardial infarction (MI) patient.

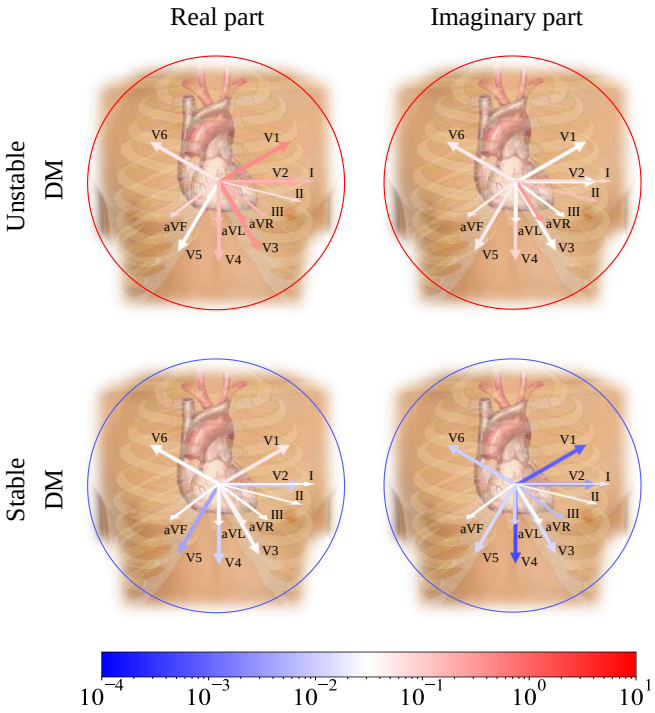

Fig. 4. The values of real and imaginary parts of single stable and unstable DMs for one ECG beat. The Arrows indicate the position of the leads. The color bar indicates the values of real and imaginary parts of each element of these DMs. Each of these elements correspond to individual lead. Note: These DMs were randomly selected from individual beat's 12-lead ECG signals of one subject for illustration.

$$\boldsymbol{\Lambda}^s = \begin{bmatrix} \lambda_1^s & 0 & \cdots & \cdots & 0 \\ 0 & \ddots & 0 & 0 & \vdots \\ \vdots & 0 & \lambda_c^s & 0 & \vdots \\ \vdots & 0 & 0 & \ddots & 0 \\ 0 & \cdots & \cdots & 0 & \lambda_C^s \end{bmatrix} \tag{16}$$

where $\boldsymbol{\phi}_c^s$ is a vector which represents stable DM and λ_c^s is the element which denotes its corresponding eigenvalue, where $c = 1,2,\ldots,C$, and C denotes the total number of stable DMs. Each element of stable DM $\boldsymbol{\phi}_c^s$, namely $\boldsymbol{\phi}_c^s(l)$, corresponds to each lead. Since the number of ECG leads (12 in this study) is always less than the number of snapshots (or time points of each beat), i.e. $12 < k$, the observed non-zero singular values given by SVD $\mathbf{X}$ is smaller than both the number of leads (12) and the total number of snapshots ($k-1$). Consequently, the maximum number of DMs is limited to 12, and these few DMs are insufficient to fully capture the dynamic activity of the cardiac system. To solve this problem, we followed the method suggested by Brunton *et al.*, which is to increase rows of the data matrix $\mathbf{X}$ to at least twice the number of columns by stacking time-shifted versions of the original signal to get an augmented data matrix $\mathbf{X}_{aug}$. It should be noted that in practical application, DMD is implemented on the augmented matrix $\mathbf{X}_{aug}$, rather than $\mathbf{X}$. The detailed steps for data augmentation are shown in the Appendix. After applying DMD on the augmented data $\mathbf{X}_{aug}$, we restacked the extracted DMs from this augmented data matrix to get DMs whose elements correspond to the 12 leads as shown in the Appendix.

C. Feature Extraction

After preprocessing, we decomposed the signal contents of each beat and frame into a set of stable and unstable DMs in each time interval, then we derived three types of features: the feature reflecting the ratio of number of unstable DMs to total DMs, the features derived from eigenvalues, and the features derived from DMs (or eigenvectors).

The first type of feature was derived in order to evaluate the ratio of unstable to total DMs as follows:

$$R_N = \frac{D}{(D+C)} \tag{17}$$

where R_N represents the ratio of unstable DMs to total DMs.

Then, we derived the parameters based on eigenvalues, because they can generally reflect information inherent to their corresponding DMs. These parameters were extracted as follows. We examined the relationship between eigenvalues of stable and unstable DMs as shown below:

$$R_\lambda = \frac{\sum_{d=1}^{D}\left|\lambda_d^u\right|}{\sum_{d=1}^{D}\left|\lambda_d^u\right| + \sum_{c=1}^{C}\left|\lambda_c^s\right|} \tag{18}$$

where R_λ represents the ratio of eigenvalue magnitudes of unstable DMs to those of total DMs. Furthermore, we examined the eigenvalue magnitudes of the most stable and unstable DMs, respectively demonstrating the fast convergent and divergent DMs, as follows:

$$\lambda_{\min} = \min\left(\left|\boldsymbol{\Lambda}^s\right|\right) \tag{19}$$

$$\lambda_{\max} = \max\left(\left|\boldsymbol{\Lambda}^u\right|\right) \tag{20}$$

where $\lambda_{\min}$ and $\lambda_{\max}$ respectively indicate the eigenvalues of the most and least stable DM.

Finally, we derived the features based on DMs (or eigenvectors). For an individual beat and frame in 12-lead ECG signals, each element of DM $\boldsymbol{\phi}_d^u$ or $\boldsymbol{\phi}_c^s$ (with the size 12×1), namely $\boldsymbol{\phi}_d^u(l)$ or $\boldsymbol{\phi}_c^s(l)$, contains two important pieces of information: the magnitude of the element (absolute value), providing a measure of the lead's participation within DM; and the phase of the element (angle between the real and imaginary components). Therefore, this study attempts to use the magnitude as well as phase of the stable and unstable DMs as useful information for the 12-lead ECG signals. We quantified the relationship between the magnitudes of stable and unstable DMD modes as follows:

$$R_M = \frac{\sum_{l=1}^{12}\sum_{d=1}^{D}\left|\boldsymbol{\phi}_d^u(l)\right|}{\sum_{l=1}^{12}\sum_{d=1}^{D}\left|\boldsymbol{\phi}_d^u(l)\right| + \sum_{l=1}^{12}\sum_{c=1}^{C}\left|\boldsymbol{\phi}_c^s(l)\right|} \tag{21}$$

where R_M represents the overall ratio of the magnitudes of the 12 leads of unstable DMD modes to total DMD modes. We also quantified how the phases of the stable DMs are related to those of unstable DMs as follows:

$$R_P = \frac{\sum_{l=1}^{12}\sum_{d=1}^{D} angle\left(\boldsymbol{\phi}_d^u(l)\right)}{\sum_{l=1}^{12}\sum_{d=1}^{D} angle\left(\boldsymbol{\phi}_d^u(l)\right) + \sum_{l=1}^{12}\sum_{c=1}^{C} angle\left(\boldsymbol{\phi}_c^s(l)\right)} \tag{22}$$

where R_P denotes the overall ratio of the oscillatory phases of the 12 leads of unstable DMs to total DMs. Furthermore, we computed the average magnitude and phase of stable DMs of each lead as shown below:

$$\boldsymbol{M}_{lead}^s = \frac{\sum_{c=1}^{C}\left|\boldsymbol{\phi}_c^s\right|}{C} \tag{23}$$

$$\boldsymbol{P}_{lead}^s = \frac{\sum_{c=1}^{C} angle\left(\boldsymbol{\phi}_c^s\right)}{C} \tag{24}$$

where both $\boldsymbol{M}_{lead}^{s}$ and $\boldsymbol{P}_{lead}^{s}$ are 12×1 vectors whose elements represent the average magnitudes and phases respectively of stable DMs of each lead. Finally, we computed the average magnitudes and phases of unstable DMs from each lead as shown below:

$$\boldsymbol{M}_{lead}^{u}=\frac{\sum_{d=1}^{D}\left|\boldsymbol{\phi}_{d}^{u}\right|}{D} \tag{25}$$

$$\boldsymbol{P}_{lead}^{u}=\frac{\sum_{d=1}^{D}angle\left(\boldsymbol{\phi}_{d}^{u}\right)}{D} \tag{26}$$

where $\boldsymbol{M}_{lead}^{u}$ and $\boldsymbol{P}_{lead}^{u}$ are also 12×1 vectors whose elements represent average magnitudes and phases respectively of unstable DMs from each lead.

Since the raw ECG signal data are strictly real values, the decomposition generates complex conjugate pairs of DMs and eigenvalues. Thus, the phases of each pair of modes are opposite to each other, and the observed results in (24) and (26) will be equal to 0. In order to solve this problem, for each DM, the phase of lead I was subtracted from the phase of each lead, then the relative phases of all DMs were averaged. It should be noted that these newly developed parameters were extracted from ECG signals in each beat as mentioned above.

D. Statistical Tests

For two-class ECG analysis, a total of 54 features extracted from the stable and unstable DMs of each ECG beat and frame for the HC group and patients with each of the mentioned pathologies (MI, CM, DT, BBB and HT) were utilized for analysis. The Jarque-Bera test was applied on each feature for normality evaluation at a significance level of 0.05. This test demonstrated that most of the extracted features were not normally distributed. Therefore, the Wilcoxon rank-sum test was implemented to investigate the DMs' stability differences between the two groups (i.e. HC group and each of the aforementioned pathologies group). The p value was considered significant if it was less than 0.05 after Bonferroni correction.

For eight-class ECG analysis, 54 features were also extracted from the stable and unstable DMs of each ECG beat and frame. Then, an analysis of variance test was conducted on each extracted feature to assess the significant differences between the DMs' stability of ECG signals (ECG beats and frames) for the normal, MI, CM, BBB, DT, HT, VHD, and MCD subjects.

E. Classification

After conducting the statistical tests, to prevent overfitting, only significant features were used to assess the performance of our proposed approach for two-class (i.e. HC group and each of the aforementioned pathologies group) and eight-class classification of ECG signals. This performance was assessed using nine commonly used classifiers: k-nearest neighbor (KNN), J48 decision tree, random forest, random tree, AdaBoost, Bayes net, vote, support vector machine (SVM), and multilayer perceptron (MLP) [48]–[56]. The open-source software WEKA was used to build these classifiers [57], and 10-fold stratified cross-validation (CV) was chosen to evaluate the performance of these models. Finally, the performance parameters of the mentioned classifiers, including accuracy, precision (or positive predictive value (PPV)), recall (or sensitivity), and area under the curve (AUC) were considered to evaluate the ability of our proposed method for ECG signal analysis.

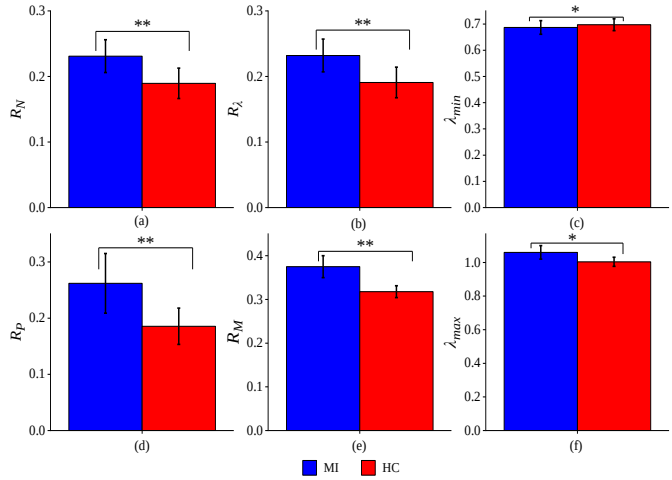

Fig. 5. The means and standard deviations of our features for MI patients and HCs. (a) R_N denotes the ratio of number of stable DMs to total DMs; (b) R_λ represents the ratio of the eigenvalue magnitudes of unstable DMs to those of all DMs; (c) $\lambda_{\min}$ denotes the eigenvalue of the most stable DM; (d) R_P represents the overall ratio of oscillatory phases of the 12 leads of unstable DMs to total DMs; and (e) R_M denotes the overall ratio of the magnitudes of 12 leads of unstable DMs to total DMs; and (f) $\lambda_{\max}$ represents the eigenvalue of the least stable DM (after Bonferroni correction, * $p<0.05$, ** $p<0.0001$).

III. Results

A. Statistical Analysis

For two-class ECG analysis, we found that out of the total of 54 features, 39 features were significant for the detection of MI, 28 for CM, 32 for DT, 26 for BBB, and 15 for HT versus the HC, using either beat-based or frame-based processing (after Bonferroni correction). Notably, the results obtained in assessing the significance of the differences between the beats and frames of the patients with each of the aforementioned pathologies and those from HCs exhibited a similar trend. Thus, we only show the results for MI detection. As illustrated in Fig. 5, MI patients generally exhibit more instability in the DMs of ECG signals compared to those from HCs. Furthermore, as shown in Fig. 6, for both MI patients and HCs, the average magnitude and phase in each lead in both stable and unstable DMs are different from those of other leads. Additionally, as shown in Fig. 6(a), most leads' stable DMs in HCs (except leads II, III, and aVF) were greater in magnitude than those from MI patients. Similarly, as shown in Fig. 6(d), except for lead II, and aVF, the other leads'

This article has been accepted for publication in a future issue of this journal, but has not been fully edited. Content may change prior to final publication. Citation information: DOI 10.1109/JBHI.2021.3130275, IEEE Journal of Biomedical and Health Informatics

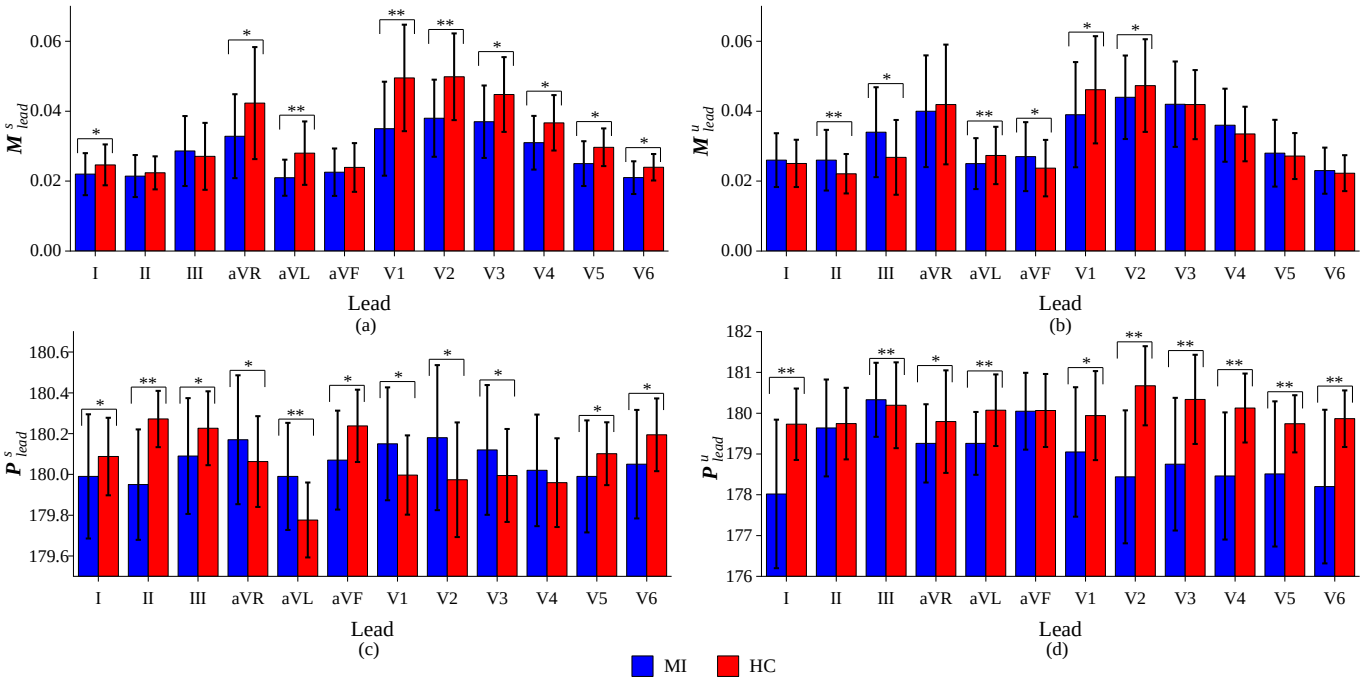

Fig. 6. The means and standard deviations of averaged magnitudes and phases of DMs of individual leads of MI patients and HCs. (a) $\boldsymbol{M}^{s}_{lead}$ represents the averaged magnitudes of stable DMs; (b) $\boldsymbol{M}^{u}_{lead}$ denotes the averaged magnitudes of unstable DMs; (c) $\boldsymbol{P}^{s}_{lead}$ denotes the averaged phases of stable DMs; and (d) $\boldsymbol{P}^{u}_{lead}$ represents the averaged phases of unstable DMs (After the Bonferroni correction, * $p<0.05$, ** $p<0.0001$)

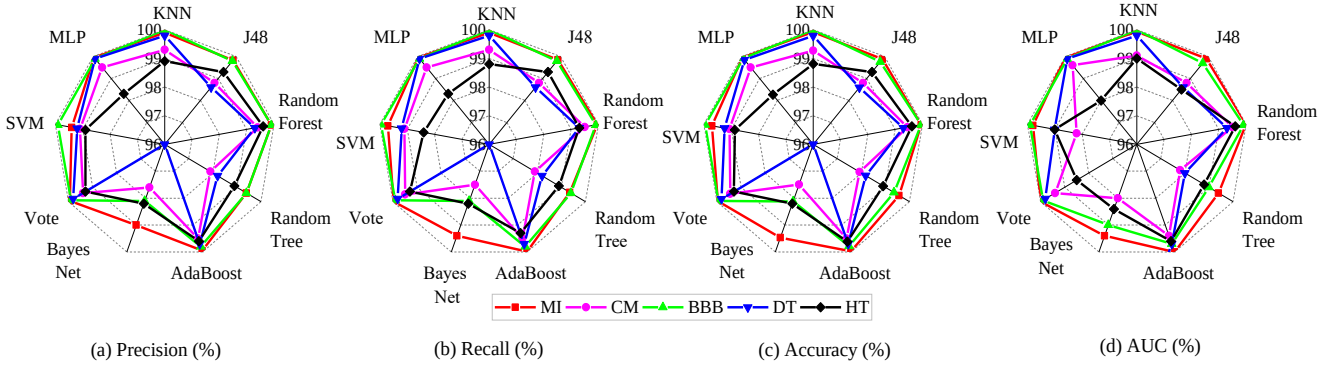

Fig. 7. Classification performance (accuracy, precision, recall, and AUC) for our features when identifying MI, CM, DT, BBB and HT from normal beats.

oscillatory phases in unstable DMs from HCs were higher than those of MI patients.

For eight-class ECG signal analysis, from the total of 54 features, 45 were significant for distinguishing the beats of those eight classes, and 39 for the frames (after Bonferroni correction).

B. Classification

As mentioned previously, 10-fold CV was used and performance parameters of the mentioned classifiers, including accuracy, PPV, sensitivity, and AUC, were considered to assess the ability of our proposed method for ECG signal analysis.

For two-class ECG signal analysis, as shown in Fig. 7 and Fig. 8, respectively, all the classifiers accurately identified the normal beats and frames from MI, CM, BBB, DT, and HT beats and frames. Specifically, the highest accuracy values achieved in detecting MI, CM, BBB, DT, and HT beats were 99.97%, 99.5%, 100%, 99.85%, and 99.61%, respectively (see Fig. 7). Accuracy values of 100%, 100%, 100%, 100%, and 99.8% were obtained for detection of MI, CM, BBB, DT, and HT frames, respectively (see Fig. 8).

As shown in Fig. 9, the classification performance achieved in the case of seven different abnormal and normal ECG signals for multiclass (eight-class) ECG signals, is consistent between beat-based and frame-based processing. Specifically,

This article has been accepted for publication in a future issue of this journal, but has not been fully edited. Content may change prior to final publication. Citation information: DOI 10.1109/JBHI.2021.3130275, IEEE Journal of Biomedical and Health Informatics

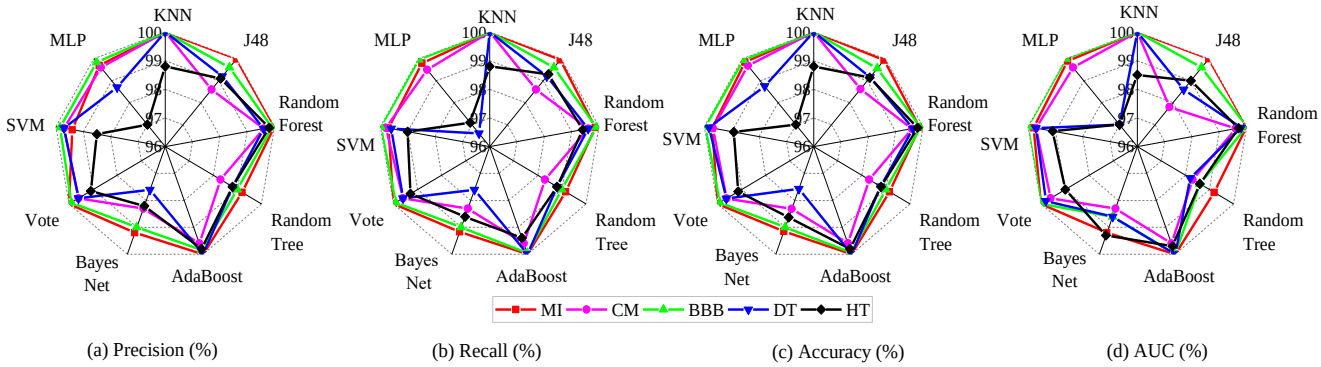

Fig. 8. Classification performance (accuracy, precision, recall, and AUC) for our features for identifying MI, CM, DT, BBB and HT frames from normal frames.

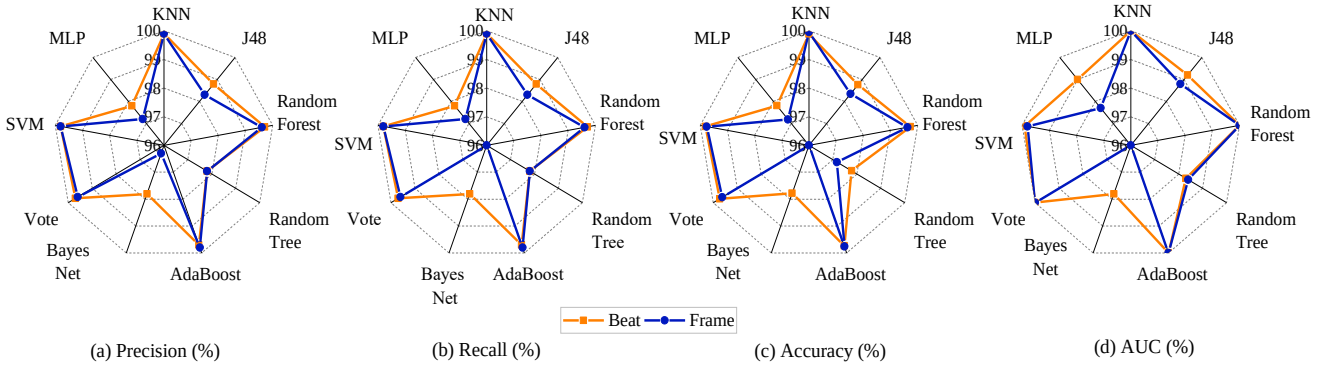

Fig. 9. The classification performance (accuracy, precision, recall, and AUC) for our developed features on multiclass (eight classes) ECG (MI, CM, DT, BBB HT, VHD, MCD and HC) beats and frames.

the highest accuracy values achieved when classifying beats and frames were 99.88% and 99.95%, respectively.

Finally, we compared our proposed approach with those of previous studies for classification of two-class and eight-class ECG signals. The highest performance achieved by these studies are summarized in Tables I and II. It is clear that our proposed method outperforms all of the existing methods.

IV. Discussion

In this study, we consider patients with different cardiac pathologies (MI, CM, DT, BBB, HT, MC, and VHD) and HCs as an example, and applied a new decomposition method, namely DMD, to decompose multi-lead ECG signals into stable and unstable modes (or subsystems). Then, we extracted the features to quantify the relationships between these two types of modes. The results verified our hypothesis that the stability of ECG modes (or subsystems) reflect the health status of individuals, which could be a new perspective for ECG signal analysis.

As mentioned in the introduction, this study has hypothesized that the stability changes of DMs in ECG signals are influenced when individuals suffer from cardiac diseases, and the results conform to the hypothesis. We extracted 54 features which reflect the relationships between stable and unstable DMs. These features can be divided into three parts: (1) Feature which reflects the proportion of number of unstable DMs to stable DMs R_N. (2) Features extracted according to eigenvalues, including R_λ, $\lambda_{\min}$, and $\lambda_{\max}$. (3) Features extracted from magnitudes and phases of eigenvectors, including R_M, R_P, $\boldsymbol{M}^s_{lead}$, $\boldsymbol{P}^s_{lead}$, $\boldsymbol{M}^u_{lead}$, and $\boldsymbol{P}^u_{lead}$. Interestingly, we found that 39, 28, 32, 26, and 15 features from total of 54 were significant for the detection of MI, CM, DT, BBB, and HT, respectively, using either beat-based or frame-based processing. This demonstrates that our proposed method can be generally effective for two-class ECG classification. Also, 45 and 39 features out of the 54 were significant for the classification of beats and frames respectively of seven cardiac pathologies. As mentioned previously, the statistical results obtained for the detection of the aforementioned pathologies (MI, CM, DT, BBB, and HT) were similar. Therefore, we only showed the results for MI detection. As illustrated in Fig. 5, greater instability in the DMs of MI patients was observed compared to those in HCs. This may be due to the presence of ECG changes (such as variation of P-wave, QRS-complex, T-wave, and ST-segment) during MI. All of these observed results conform to findings from previous studies, which state that changes in the stability of physiological signals reflect individuals' pathological conditions. In addition, according to the theory of cybernetics, stable subsystems can generally assist the whole system to work more efficiently, orderly, and adaptive, while unstable

TABLE I
PERFORMANCE COMPARISON OF THE PROPOSED METHOD WITH EXISTING APPROACHES USED THE PTB ECG DATABASE FOR DETECTION OF ECG PATHOLOGIES

Method	# Leads	Disease and # Beat/ frame	Acc. (%)	PPV (%)	Sens. (%)	AUC (%)
DWT [28]	1(II)	2282 MI & 718 HC beats	96.93	N/R	N/R	N/R
ST-segment analysis [26]	12	20 MI & 20 HC records	N/R	N/R	85	N/R
Time-domain analysis [21]	12	16960 MI & 3200 HC beats	98.30	N/R	99.97	N/R
Multiple-instance learning on ST-segment [27]	12	369 MI &79 HC records	N/R	N/R	92.30	N/R
Polynomial function and DWT [29]	12	148 MI & 52 HC subjects	94.40	N/R	N/R	N/R
WT and multiscale energy and eigenspace [30]	12	2148 MI &2148 HC frames	96	N/R	93	96.16
- Variability of T-wave amplitude [13] - Variability of T-wave angle - Variability of QT-interval	1 (II)	79 MI & 69 HC records	N/R N/R N/R	N/R N/R N/R	N/R N/R N/R	85 95 83
-DCT [23] -DWT -EMD	1 (II)	40182 MI & 10546 HC beats	98.50 98.16 81.34	99.8 99.77 93.96	99.70 99.69 97.23	N/R N/R N/R
Shallow CNN [33]	3 (II, III, aVF)	30 MI & 52 HC subjects	84.54	N/R	85.33	N/R
CNN and RNN [34]	12	148 MI & 52 HC subjects	N/R	97.20	92.40	N/R
DFT [22]	3 (II, III, V2)	15000 MI & 5000 HC beats	95.60	N/R	96.50	N/R
Time-domain analysis and PCA [24]	12	60 MI & 60 HC records	96.96	N/R	96.96	N/R
Optimal band filtering bank and WT [31]	1	40182 MI & 10546 HC beats	99.74	99.80	99.84	100
ST segment, T and Q waves analysis [25]	12	113 MI & 52 HC subjects	99.80	N/R	99.75	N/R
Maximal overlap DWT [32]	12	21569 MI & 7131 HC	99.57	N/R	99.82	N/R
Principal component multivariate multiscale sample entropy [35]	12	-135 CM & 140 HC -63 HT & 140 HC -99 DT & 140 HC	93.03 85.29 90.09	N/R N/R N/R	N/R N/R N/R	N/R N/R N/R
Complex wavelet sub-band bi-spectrum [36]	12	-352 BBB & 352 HC frames	96.40	N/R	N/R	N/R
Application of specific signal processing for integrated circuits [37]		-7 HT & 52 HC subjects -14 DT & 52 HC subjects -15 BBB & 52 HC subjects	99.31 99.66 99.31	N/R N/R N/R	N/R N/R N/R	N/R N/R N/R
Stability analysis of dynamic modes of ECG signals by DMD	**12**	**Beats:** **-35010 MI & 10140 HC** **-2591 CM & 10140 HC** **-1091 HT & 10140 HC** **-1203 DT & 10140 HC** **-2456 BBB & 10140 HC** **Frames:** **-8727 MI & 2496 HC** **-693 CM & 2496 HC** **-287 HT & 2496 HC** **-468 DT & 2496 HC** **-672 BBB & 2496 HC**	 **99.97±0.02** **99.50±0.10** **99.61±0.18** **99.85±0.07** **100** **100** **100** **99.80±0.15** **100** **100**	 **99.96±0.02** **99.50±0.36** **99.60±0.10** **99.90±0.08** **100** **100** **100** **99.80±0.15** **100** **100**	 **99.96±0.02** **99.50±0.33** **99.30±0.18** **99.90±0.05** **100** **100** **100** **99.4±0.16** **100** **100**	 **100** **99.60±0.10** **99.60±0.20** **99.90±0.08** **100** **100** **100** **99.70±0.13** **100** **100**

Note: #: number; &: and; Acc.: accuracy; PPV: positive predictive value; Sens.: sensitivity; N/R: not reported; WT: wavelet transform; DWT: discrete wavelet transform; DCT: discrete cosine transform; EMD: empirical mode decomposition; DFT: discrete Fourier transform; PCA: principal component analysis; CNN: convolution neural network, and RNN: recurrent neural network. It should be also noted that confidence intervals obtained by these methods were not reported.

subsystems are almost the opposite. This study has found a similar phenomenon in the cardiac system - that is, the DMs of HCs are less stable compared to those of MI patients, which indicates that their cardiac systems function in a more efficient, orderly, and adaptive manner than those of MI patients. However, we also found some interesting phenomena: (1) As shown in Fig. 6, for both stable and unstable DMs, the magnitudes and phases of different leads vary from each other. This demonstrates that different leads can convey different useful information for disease diagnosis, hence it is meaningful to analyze these leads separately. (2) Furthermore, our results ascertain that most leads of HCs in stable DMs (except lead II, III, and aVF) exhibit larger magnitudes compared with those of MI patients (see Fig. 6(a)). This demonstrates that the leads in stable DMs of HCs are more active compared to those of MI patients, which can reflect the normal and sufficient adaptability of their cardiac systems.

(3) Similarly, as illustrated in Fig. 6(d), most leads of HCs in unstable DMs (except lead II and aVF) exhibit higher oscillatory phases compared to those of MI patients. This may be because the cardiac systems of healthy individuals are capable of detecting and responding quickly to any changes subjected to them. (4) We also found that the average phases for some leads in stable DMs, such as II, III, aVF, and V4, for the MI patient group differed significantly from those in the

TABLE II
PERFORMANCE COMPARISON OF THE PROPOSED METHOD WITH EXISTING APPROACHES USED THE PTB ECG DATABASE FOR MULTICLASS ECG SIGNAL CLASSIFICATION

Method	# Leads	Number of ECG classes	Acc. (%)	Sens. (%)
Principal component multivariate multiscale sample entropy [35]	12	5 (140 HC, 144 MI, 135 CT, 99 DT, and 63 HT frames of 4.096 seconds)	90.34	N/R
Dual tree complex wavelet transform [38]	12	4 (352 HC, 352 MI, 352 BBB, and 420 HMD (or CT and HT) frames of 4.096 seconds	86.09	86.41
CNN and radial basis function neural networks [39]	12	8 (total of 1056 frames of 20 seconds from 52 HC, 148 MI, 15 BBB, 18 CT, 14 DT, 7 HT, 4 MC, and 6 VHD subjects)	94.35	N/R
CNN and bidirectional long short-term memory [40]	12	3 (1588 HC, 7390, MI, and 1353 non-MI (or BBB, CT, DT, HT, MC, and VHD) frames of 12 consecutive beats	99.25	99.25
Stability analysis of dynamic modes of ECG signals by DMD	**12**	**8 (2496 HC, 8727 MI, 672 BBB, 693 CM, 468 DT, 287 HT, 93 MC, and 131 VHD frames of 4.096 seconds)**	**99.95**	**99.90**

Note: #: number; Acc.: accuracy; Sens.: sensitivity; N/R: not reported; It is also worth noting that the precision and AUC values achieved by these studies were not reported.

HC group. However, the average magnitudes of those leads were not significant (see Fig. 6(a) and (c)). Similarly, the average phases for some leads in unstable DMs, such as I, aVR, aVF, V3, V4, V5, and V6, differed significantly between the two groups. However, the average magnitudes of those leads were not significant (see Fig. 6(b) and Fig. 6(d)). This demonstrates that the phase and magnitude of individual leads contain different information, thus they all need to be considered when analyzing stable and unstable DMs.

In order to further investigate the effectiveness of our proposed approach in differentiating two and eight groups, nine classifiers were implemented, because each of them utilizes distinct techniques for data classification. Encouragingly, as shown in Fig. 7, each of the classifiers was able to accurately identify MI, CM, BBB, DT, and HT beats from those of HCs, with respective highest accuracy values of 99.97%, 99.5%, 100%, 99.85%, and 99.61%. Also, 100% accuracy was obtained for the detection of MI, CM, BBB, and DT frames (see Fig. 8). Similarly, the highest accuracy values of 99.88% and 99.95% were respectively achieved when classifying beats and frames of multiple heart pathologies (MI, CM, BBB, DT, MC, VHD, and HT) (see Fig. 9). Furthermore, we also summarized the results from previous studies for the classification of two-class and multiclass ECG signals, for comparison with our observed results (see Tables I and II). Interestingly, our proposed approach outperformed all of the existing approaches; in other words, this demonstrates the potential of our proposed approach for ECG signal analysis, helping cardiologists to enhance the automated diagnosis of different cardiac pathologies. Additionally, it should be noted that our method was compared with a previous study which used univariate ECG signal analysis (single-lead ECG) in terms of storage and complexity [31]. We used a computer with Intel CORE 2.4 GHz (i5–4210U) processor and 4 GB RAM. The execution times used for feature extraction and detection of MI (KNN classifier, training and testing using 10-fold CV as in [31]) were 14.14 seconds and 30.06 seconds, respectively. The execution time of [31] was considerably less, and their proposed method is good, but our proposed method is still the best. Also, the performance of our proposed method was evaluated for detection of other four cardiac pathologies. The classification of these pathologies achieved promising results. However, the method of Sharma *et al.* has not yet been tested for detection of other heart pathologies, we are not certain if their method is also suitable for detecting other heart diseases, or for multiclass ECG signal classification [31].

It should also be noted that in order to conveniently and objectively compare our proposed approach with the existing approaches, we repeated the strategies of most previous studies which used the PTB dataset. These strategies involve preprocessing and use of 12-lead ECG signals in the analysis. However, to further demonstrate the improvement of our proposed approach, we used MI as an example and included two supplementary evaluations: (1) we evaluated our proposed method on 9-lead ECG signals after removing some leads (augmented leads aVR, aVL, and aVF) to reduce the effect of the data redundancy in leads I, II, III, aVR, aVL, and aVF, which may affect our conclusion. The observed results were consistent with those obtained on 12-lead ECG signals. We have reported the results of 12-lead ECG signals for comparison; but in the future, we might also use 9-lead ECG signals to reduce computation time. (2) To assess our denoising performance, we evaluated the performance of our proposed method on noisy ECG signals, obtaining respective highest accuracy, precision, recall, and AUC values of 99.94%, 99.92%, 99.94%, and 99.93%. This demonstrates the robustness of our proposed method in the case of noisy signals, and can be useful in clinical data, which often suffer from noise and artifacts. However, compared with noisy ECG signals, we achieved the highest classification performance on preprocessed ECG signals. This indicates good denoising performance on ECG signals.

Several further points also need to be mentioned. (1) As mentioned before, the Pan-Tompkins algorithm is commonly used for R-peak detection [43]. Although it is not optimal, it can achieve the promising accuracy of 99.32% and is currently regarded as one of the best approaches for detection of R-peaks [40]. Some R-peaks cannot be accurately detected by the algorithm, but our proposed approach can still achieve the highest performance for the classification of cardiac pathologies. This demonstrates the robustness of our proposed method for cardiac disease diagnosis. (2) Regarding fast Fourier transform (FFT), the power spectrum of each

frequency point contains magnitude and phase information. Similarly, DMD can be regarded as a new way to calculate the spectra of multivariate signals, but it is not the same as FFT (which is used for univariate signals). In this study, we calculated the phase, which has a totally different physiological meaning from that of leads in raw ECG signals. Specifically, we computed the phase of DMs (which can be regarded as subsystems) of ECG signals. (3) The DMD algorithm revealed the amplitude variation of two neighbor points, then accurately uncovered the shape of each ECG wave, revealing the relationship among ST-segment, P-wave, T-wave, and QRS complex. Therefore, DMD can be considered as another technique for ECG morphological analysis. (4) In the PTB database, apart from MI patients, most normal, CM, BBB, DT, HT, MCD, and VHD subjects have one ECG recording. Thus, we randomly selected one ECG recording for each subject. In order to compare our method with the MI detection methods in [23] and [31], we followed their strategies, using 40182 MI and 10546 HC beats, achieving the highest accuracy, PPV, sensitivity, and AUC values of 99.95%, 99.93%, 99.95%, and 99.94%, respectively. These observed results are consistent with those for 35010 MI and 10140 HC beats.

Finally, the major contributions of our proposed approach can be summarized as follows. (1) We are the first to use dynamic mode decomposition (DMD) to evaluate how the stability of ECG modes (or subsystems) affects the macrodynamic patterns of multilead ECG signals. No one used this stability concept to analyze physiological signals. The results show that this stability is an inherent phenomenon for all mentioned types of cardiac pathologies. Therefore, our proposed method can reveal new cardiac mechanisms, which cannot be achieved by other existing methods and can effectively help in disease diagnosis. Thus, it might be used in clinical studies. (2) In addition, in contrast to other traditional data decomposition methods, such as PCA, EMD, and WT, only DMD can decompose high-dimensional and dynamic data into subsystems, namely DMs, with stability. Therefore, this study is the first attempt to analyze ECG signals based on stable and unstable DMs of multi-lead ECG signals, which may not only help to reveal new cardiac dynamic mechanisms, but also contribute to research on heart-related diseases. (3) DMD was initially implemented in the analysis of fluid flows and has recently been used in analysis of high-dimensional and dynamic physiological signals and public health data, such as epidemiological data, brain-related signals, and others [15]–[19]. However, DMD has not yet been used to analyze multi-lead ECG signals, which are also dynamic and high-dimensional. (4) Additionally, we evaluated the performance of our proposed method for the detection of five cardiac pathologies (MI, DT, BBB, CT, and HT) and achieved promising results. (5) Also, the highest classification performance was achieved for the classification of eight ECG signals (normal and seven abnormal groups, which cover most of the main types of ECG signals). This demonstrates the robustness and generalizability of our proposed method for heart disease diagnosis. (6) Apart from that, our proposed method was able to accurately detect different cardiac pathologies using beat-based and frame-based processing, which demonstrates that our proposed method can extract the essential information for heart disease diagnosis without being affected by processing technique.

Since DMD is a multivariate analysis approach which has the advantage of being able to simultaneously analyze the ECG signals of all leads and automatically reflect the relationship between them. Thus, it may be difficult to implement it in wearable devices, which normally have either single or dual leads. Thus, our method might be more suitable in clinics.

V. Conclusion

In this study, we proposed a novel perspective for the analysis of ECG signals, which relies on the stability analysis of ECG subsystems by decomposing ECG signals into stable and unstable modes using DMD. Furthermore, this study also demonstrates that the stability analysis of ECG modes (or subsystems) can reveal the underlying spatiotemporal dynamics of the cardiac system, and reflects the heart condition status of an individual. Finally, our proposed method exhibits great potential as well as high accuracy for diagnosis of heart disease, and might be widely applied in clinical studies as well as various engineering-related applications. In future, our proposed approach should be applied to other physiological signals, such as brain-related and electromyography signals, to evaluate the stability of their DMs (or subsystems). This can help clinicians to comprehensively understand their underlying mechanisms and diagnose their related diseases.

Appendix

Data Matrices Augmentation for DMD

As mentioned in the method part section B, for implementing DMD on the 12-lead ECG data, the raw data matrix $\mathbf{X}$ must be augmented to get new augmented matrix $\mathbf{X}_{aug}$ so that the extracted DMs can fully capture the underlying dynamics over k snapshots. This augmented matrix $\mathbf{X}_{aug}$ was constructed by extending the snapshot measurements with $q-1$ time-shifted versions of their own. Therefore, the number of measurements is augmented to qn (or $12q$). In this study, the smallest possible integer q was chosen so that $qn \geq 2k$ as recommended in [14].

In this study, we implemented DMD on each beat with 651 samples. Since ECG data has 12 leads, then the values for parameters k, and q are 651, and 109, respectively. The augmented data matrix $\mathbf{X}_{aug}$ is shown below:

$$\mathbf{X}_{aug} = \begin{bmatrix} \mathbf{x}_1 & \mathbf{x}_2 & \cdots & \mathbf{x}_{k-q} \\ \mathbf{x}_2 & \mathbf{x}_3 & \cdots & \mathbf{x}_{k-q+1} \\ \vdots & \vdots & \vdots & \vdots \\ \mathbf{x}_q & \mathbf{x}_{q+1} & \cdots & \mathbf{x}_{k-1} \end{bmatrix} \tag{27}$$

where $\mathbf{x}_{k-1}$ is 12×1 vector containing the measurements from 12 leads of ECG signals at each time interval. Since $\mathbf{x}_{k-1}$ is 12×1 vector, then the observed $\mathbf{X}_{aug}$ is 1308×542 matrices.

After, DMD was implemented on augmented data $\mathbf{X}_{aug}$ to get DMs (stable and unstable DMs). The DMs extracted from this augmented data matrix are shown below:

$$\mathbf{\Phi}^{u}_{stacked}=\begin{bmatrix}\boldsymbol{\phi}^{u}_{11} & \boldsymbol{\phi}^{u}_{12} & \cdots & \boldsymbol{\phi}^{u}_{1D}\\ \boldsymbol{\phi}^{u}_{21} & \boldsymbol{\phi}^{u}_{22} & \cdots & \boldsymbol{\phi}^{u}_{2D}\\ \vdots & \vdots & \vdots & \vdots\\ \boldsymbol{\phi}^{u}_{q1} & \boldsymbol{\phi}^{u}_{q2} & \cdots & \boldsymbol{\phi}^{u}_{qD}\end{bmatrix}=\left[\boldsymbol{\phi}^{u}_{1stacked},\boldsymbol{\phi}^{u}_{2stacked},\ldots,\boldsymbol{\phi}^{u}_{Dstacked}\right] \quad (28)$$

$$\mathbf{\Phi}^{s}_{stacked}=\begin{bmatrix}\boldsymbol{\phi}^{s}_{11} & \boldsymbol{\phi}^{s}_{12} & \cdots & \boldsymbol{\phi}^{s}_{1C}\\ \boldsymbol{\phi}^{s}_{21} & \boldsymbol{\phi}^{s}_{22} & \cdots & \boldsymbol{\phi}^{s}_{2C}\\ \vdots & \vdots & \vdots & \vdots\\ \boldsymbol{\phi}^{s}_{q1} & \boldsymbol{\phi}^{s}_{q2} & \cdots & \boldsymbol{\phi}^{s}_{qC}\end{bmatrix}=\left[\boldsymbol{\phi}^{s}_{1stacked},\boldsymbol{\phi}^{s}_{2stacked},\ldots,\boldsymbol{\phi}^{s}_{Cstacked}\right] \quad (29)$$

where q is equal to 109 and denotes the total number of stacks. $\boldsymbol{\phi}^{u}_{qD}$ and $\boldsymbol{\phi}^{s}_{qC}$ are 12×1 vectors which represent the subcomponents of unstable and stable DMs of the augmented data, respectively. $\boldsymbol{\phi}^{u}_{Dstacked}$ and $\boldsymbol{\phi}^{s}_{Cstacked}$ are the 1308×1 vectors correspond to each column of matrices $\mathbf{\Phi}^{u}_{stacked}$ and $\mathbf{\Phi}^{s}_{stacked}$, and represent unstable and stable DMs of the augmented data $\mathbf{X}_{aug}$, respectively. C and D denotes the total number of stable and unstable DMs, respectively.

After, unstable and stable DMs $\boldsymbol{\phi}^{u}_{Dstacked}$ and $\boldsymbol{\phi}^{s}_{Cstacked}$ extracted from the augmented data matrix $\mathbf{X}_{aug}$ were restacked by averaging their subcomponents to get unstable and stable DMs $\boldsymbol{\phi}^{u}_{Drestacked}$ and $\boldsymbol{\phi}^{s}_{Crestacked}$ with size of 12×1, so that their elements correspond to 12 leads as follow:

$$\mathbf{\Phi}^{u}_{restacked}=\left[\frac{\boldsymbol{\phi}^{u}_{11}+\ldots+\boldsymbol{\phi}^{u}_{q1}}{q},\frac{\boldsymbol{\phi}^{u}_{12}+\ldots+\boldsymbol{\phi}^{u}_{q2}}{q},\ldots,\frac{\boldsymbol{\phi}^{u}_{1D}+\ldots+\boldsymbol{\phi}^{u}_{qD}}{q}\right] \quad (30)$$
$$=\left[\boldsymbol{\phi}^{u}_{1restacked},\ldots,\boldsymbol{\phi}^{u}_{Drestacked}\right]$$

$$\mathbf{\Phi}^{s}_{restacked}=\left[\frac{\boldsymbol{\phi}^{s}_{11}+\ldots+\boldsymbol{\phi}^{s}_{q1}}{q},\frac{\boldsymbol{\phi}^{s}_{12}+\ldots+\boldsymbol{\phi}^{s}_{q2}}{q},\ldots,\frac{\boldsymbol{\phi}^{s}_{1C}+\ldots+\boldsymbol{\phi}^{s}_{qC}}{q}\right] \quad (31)$$
$$=\left[\boldsymbol{\phi}^{s}_{1restacked},\ldots,\boldsymbol{\phi}^{s}_{Crestacked}\right]$$

ACKNOWLEDGMENT

This work was sponsored by the National Natural Science Foundation of China (Grant number: 62171109, 61872405) and the Key R&D Project of Sichuan Province (2020YFS0094, 2020YFS0243). We also thank the support from University of Electronic Science and Technology of China.

REFERENCES

[1] G. Guven *et al.*, "Biometric identification using fingertip electrocardiogram signals," *Signal, Image Video Process.*, vol. 12, no.5, pp. 1–8, Jan. 2018.

[2] A. L. Goldberger, Ed., "Clinical electrocardiography: a Simplified Approach ," Seventh Ed., Philadelphia: Mosby, 2006, pp. 329–337.

[3] J. A. Drezner *et al.*, "Abnormal electrocardiographic findings in athletes: recognising changes suggestive of cardiomyopathy," *Br. J. Sports Med.*, vol. 47, no. 3, pp. 137–152, Feb. 2013.

[4] K. Thygesen *et al.*, "Third universal definition of myocardial infarction," *Circulation*, vol. 126, no. 16, pp. 2020–2035, Jun. 2012 .

[5] R. C. Dorf and R. C. Bishop, "Modern control systems," IEEE Trans. Syst., Man, Cybern.Syst., vol.11, no.8, pp.580, 2011.

[6] P. Kundur *et al.*, "*Power system stability and control*," New York, NY, USA: McGraw-Hill, 1994.

[7] M. V. Cook, "Flight dynamics principles: a linear systems approach to aircraft stability and control," Butterworth-Heinemann, 2012.

[8] F. Tahami *et al.*, "A novel driver assist stability system for all-wheel-drive electric vehicles," *IEEE Trans. Veh. Technol.*, vol. 52, no. 3, pp. 683–692, May. 2003.

[9] L. A. Aguirre and Á. V. P. Souza, "Stability analysis of sleep apnea time series using identified models: A case study," *Comput. Biol. Med.*, vol. 34, no. 3, pp. 241–257, Apr. 2004.

[10] G. Hocepied *et al.*, "Stability analysis of epileptic EEG signals," in *8th IEEE Int. Conf. BIBE*, 2008, pp. 1–5.

[11] L. Glass and M. C. Mackey, "Pathological conditions resulting from instabilities in physiological control systems," *Ann. N. Y. Acad. Sci.*, vol. 316, no. 1, pp. 214–235, Feb. 1979.

[12] J. Lunze, "Stability analysis of large-scale systems composed of strongly coupled similar subsystems," *Automatica*, vol. 25, no. 4, pp. 561–570, Jul. 1989.

[13] M. A. Hasan *et al.*, "Increased beat-To-beat T-wave variability in myocardial infarction patients," *Biomed. Eng.*, vol. 63, no. 2, pp. 123–130, Nov. 2018.

[14] K. K. Chen *et al.*, "Variants of dynamic mode decomposition: Boundary condition, Koopman, and fourier analyses," *J. Nonlinear Sci.*, vol. 22, no. 6, pp. 887–915, Dec. 2012.

[15] C. W. Rowley *et al.*, "Spectral analysis of nonlinear flows," *J. Fluid Mech.*, vol. 641, pp. 115–127, Sep. 2009.

[16] J. L. Proctor and P. A. Eckhoff, "Discovering dynamic patterns from infectious disease data using dynamic mode decomposition," *Int. Health*, vol. 7, no. 2, pp. 139–145, Nov. 2015.

[17] B. W. Brunton *et al.*, "Extracting spatial-temporal coherent patterns in large-scale neural recordings using dynamic mode decomposition," *J. Neurosci. Methods*, vol. 258, pp. 1–15, Jan. 2016.

[18] M. S. J. Solaija *et al.*, "Dynamic mode decomposition based epileptic seizure detection from scalp EEG," *IEEE Access*, vol. 6, no. 38683–38692, Jul. 2018.

[19] J. Casorso *et al.*, "Dynamic mode decomposition of resting-state and task fMRI," *NeuroImage*, vol. 194, pp. 42–54, Mar. 2019.

[20] World Health Organization, "Global Health Estimates 2015: Deaths by Cause, Age, Sex, by Country and by Region, 2000-2015," WHO, Geneva, 2016.

[21] M. Arif *et al.*, "Detection and localization of myocardial infarction using K-nearest neighbor classifier," *J. Med. Syst.*, vol. 36, no. 1, pp. 279–289, Mar. 2012.

[22] D. Sadhukhan *et al.*, "Automated identification of myocardial infarction using harmonic phase distribution pattern of ECG Data," *IEEE Trans. Instrum. Meas.*, vol. 67, no. 10, pp. 2303–2313, Oct. 2018.

[23] U. R. Acharya *et al.*, "Automated characterization and classification of coronary artery disease and myocardial infarction by decomposition of ECG signals: A comparative study," *Inf. Sci.*, vol. 377, pp. 17–29, Jan. 2017.

[24] A. K. Dohare *et al.*, "Detection of myocardial infarction in 12 lead ECG using support vector machine," *Appl. Soft Comput.*, vol. 64, pp. 138–147, Mar. 2018.

[25] B. Halder *et al.*, "Classification of complete myocardial infarction using rule-based rough set method and rough set explorer system," *IETE J. Res.*, Apr. 2019.

[26] S. G. Al-Kindi *et al.*, "Towards real-time detection of myocardial infarction by digital analysis of electrocardiograms," in *1st MECBME*, 2011, pp. 454–457.

[27] L. Sun *et al.*, "ECG analysis using multiple instance learning for myocardial infarction detection," *IEEE Trans. Biomed. Eng.*, vol. 59, no. 12, pp. 3348–3356, Aug. 2012.

[28] E. S. Jayachandran *et al.*, "Analysis of myocardial infarction using discrete wavelet transform," *J. Med. Syst.*, vol. 34, no. 6, pp. 985–992, May. 2010.

[29] B. Liu *et al.*, "A novel electrocardiogram parameterization algorithm and its application in myocardial infarction detection," *Comput. Biol.*

Med., vol. 61, pp. 178–184, Jun. 2015.
[30] L. N. Sharma *et al.*, "Multiscale energy and eigenspace approach to detection and localization of myocardial infarction," *IEEE Trans. Biomed. Eng.*, vol. 62, no. 7, pp. 1827–1837, July. 2015.
[31] M. Sharma *et al.*, "A novel automated diagnostic system for classification of myocardial infarction ECG signals using an optimal biorthogonal filter bank," *Comput. Biol. Med*, vol. 100, pp. 100–113, Nov. 2018.
[32] Z. Lin *et al.*, "Automated detection of myocardial infarction using robust features extracted from 12-lead ECG," *Signal, Image Video Process.*, vol. 14, pp. 857–865, Jul. 2020.
[33] T. Reasat and C. Shahnaz, "Detection of inferior myocardial infarction using shallow convolutional neural networks," in *5th IEEE R10-HTC*, 2017, pp. 718–721.
[34] W. Liu *et al.*, "Real-time multilead convolutional neural network for myocardial infarction detection," *IEEE J. Biomed. Health Inform.*, vol. 22, no. 5, pp. 1434–1444, Sep. 2018.
[35] R. K. Tripathy *et al.*, "A new way of quantifying diagnostic information from multilead electrocardiogram for cardiac disease classification," *Healthcare Technol. Lett.*, vol. 1, no. 4, pp. 98–103, Oct. 2014.
[36] R. K. Tripathy and S. Dandapat, "Automated detection of heart ailments from 12-lead ECG using complex wavelet sub-band bi-spectrum features," *Healthcare Technol. Lett.*, vol. 4, no. 2, pp. 57–63, Apr. 2017.
[37] S. K. Jain and B. Bhaumik, "An Energy Efficient ECG Signal Processor Detecting Cardiovascular Diseases on Smartphone," *IEEE trans. Biomed. Circuits Syst.*, vol. 11, no. 2, pp. 314–323, Apr. 2017.
[38] R. K. Tripathy and S. Dandapat, "Detection of cardiac abnormalities from multilead ECG using multiscale phase alternation features," *J. Med. Syst.*, vol. 40, no. 6, p. 143, Jun. 2016.
[39] M. Deng *et al.*, "Extracting cardiac dynamics within ECG signal for human identification and cardiovascular diseases classification," *Neural Netw.*, vol. 100, pp. 70–83, 2018.
[40] M. Dey *et al.*, "Temporal feature-based blassification into myocardial infarction and other CVDs merging CNN and Bi-LSTM from ECG signal," *IEEE Sensors J.*, vol. 21, no. 19, pp. 21688–21695, 2021.
[41] A. L. Goldberger *et al.*, "PhysioBank, PhysioToolkit, and PhysioNet: components of a new research resource for complex physiologic signals," *Circulation*, vol. 101, pp. 215–220, Jun. 2000.
[42] J. P. Martínez *et al.*, "A wavelet-based ECG delineator evaluation on standard databases," *IEEE Trans. Biomed. Eng.*, vol. 51, no. 4, pp. 570–581, Apr. 2004.
[43] J. Pan and W. J. Tompkins, "A Real-Time QRS Detection Algorithm," *IEEE Trans. Biomed. Eng.*, vol. 32, no. 3, pp. 230–236, Mar. 1985.
[44] E. A. Whitsel *et al.*, "RR interval variation, the QT interval index and risk of primary cardiac arrest among patients without clinically recognized heart disease," *European Heart J.*, vol. 22, no. 2, pp. 165–173, Jan. 2001.
[45] J. H. Tu *et al.*, "On dynamic mode decomposition: Theory and applications," *ACM J. Comput. Dyn.*, vol. 1, no. 2, pp. 391–421, Jun. 2014.
[46] M. H. Hayes, *Schaum Outline of Digital Signal Processing*. 1998.
[47] K. Lehnertz *et al.*, "State-of-the-art of seizure prediction," *J. Clin. Neurophysiol.*, vol. 24, no. 2, pp. 147–153, Apr. 2007.
[48] T. M. Cover and P. E. Hart, "Nearest neighbor pattern classification," *IEEE Trans. Inf. Theory*, vol. 13, no. 1, pp. 21–27, Jan. 1967.
[49] U. Bashir and M. Chachoo, "Performance evaluation of J48 and bayes algorithms for intrusion detection system," *Int. J. Netw. Secur. Appl.*, vol. 9, no. 4, Jul. 2017.
[50] A. Liaw and M. Wiener, "Classification and regression by random forest," *R News*, vol. 2, no. 3, pp. 18–22, Dec. 2002.
[51] A. Cutler and G. Zhao, "Pert - perfect random tree ensembles," *Comput. Sci. Stat.*, vol. 33, pp. 490–497, Jan. 2001.
[52] W. Hu *et al.*, "AdaBoost-based algorithm for network intrusion detection," *IEEE Trans. Syst., Man, Cybern. B. Cybern.*, vol. 38, no. 2, pp. 577–583, Apr. 2008.
[53] N. Friedman *et al.*, "Bayesian network classifiers," *Machine Learning*, vol. 29, no. 2–3, pp. 131–163, Nov. 1997.
[54] R. E. Schapire *et al.*, "Boosting the margin: A new explanation for the effectiveness of voting methods," *Ann. Stat.*, vol. 26, no. 5, pp. 1651–1686, 1998.
[55] J. A. K. Suykens and J. Vandewalle, "Least squares support vector machine classifiers," *Neural Process. Lett.*, vol. 9, no. 3, pp. 293–300, Jan. 1999.
[56] S. K. Pal and S. Mitra, "Multilayer perceptron, fuzzy sets, and classification," *IEEE Trans. Neural Netw.*, vol. 3, no. 5, pp. 683–697, Sep. 1992.
[57] E. Frank *et al.*, "Weka-a machine learning workbench for data mining," in *Data Min. Knowl. Discov., Springer*, 2009, pp. 1269–1277.